

Nº 179727

Influence of microstructure on the formation of corrosion products of steels susceptible to SCC-CO₂

**Guilherme Henrique Alves Andrade
Carlos Alberto da Silva
Zehbour Panossian**

*Palestra apresentada no
CONGRESSO
INTERNACIONAL DE
CORROSÃO, INTERCORR,
10., 2025, São Paulo. 24
slides*

“Comunicação Técnica” compreende trabalhos elaborados por técnicos do IPT, apresentados em eventos, publicados em revistas especializadas ou quando seu conteúdo apresentar relevância pública. **PROIBIDO REPRODUÇÃO**



8 A 11 DE JULHO

INTERCORR
ABRACO 2025

CDI - Centro de Difusão Internacional - USP

Influence of Microstructure on the Formation of Corrosion Products of Steels Susceptible to SCC-CO₂

Guilherme Henrique Alves Andrade – FIPT/IPT



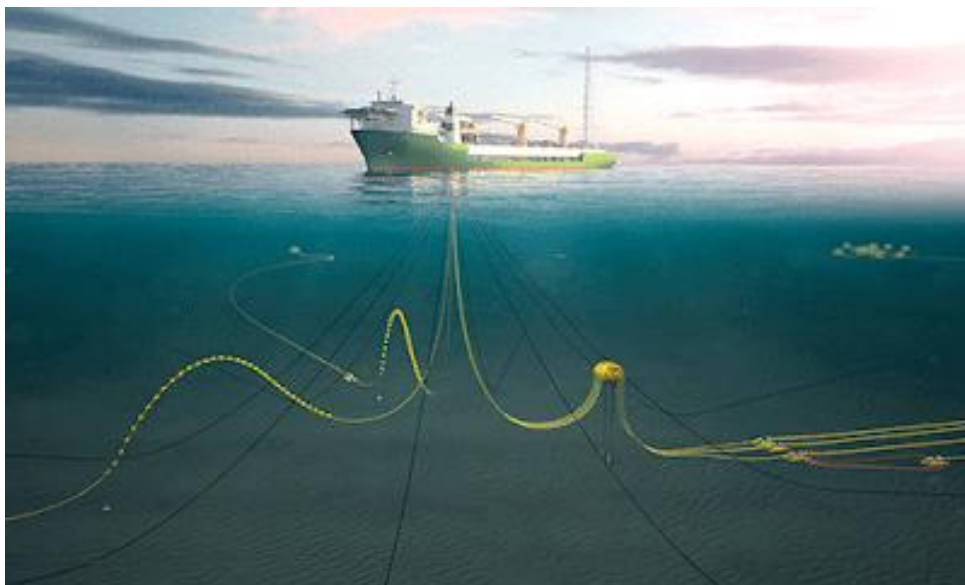


Authors:

- Guilherme Henrique Alves Andrade – FIPT/IPT
eng.mec.guilhermeandrade@gmail.com
- Carlos Alberto da Silva – FIPT/IPT
callbertt@gmail.com
- Zehbour Panossian – IPT
zep@ipt.br

InterCorr2025_233

INTRODUCTION

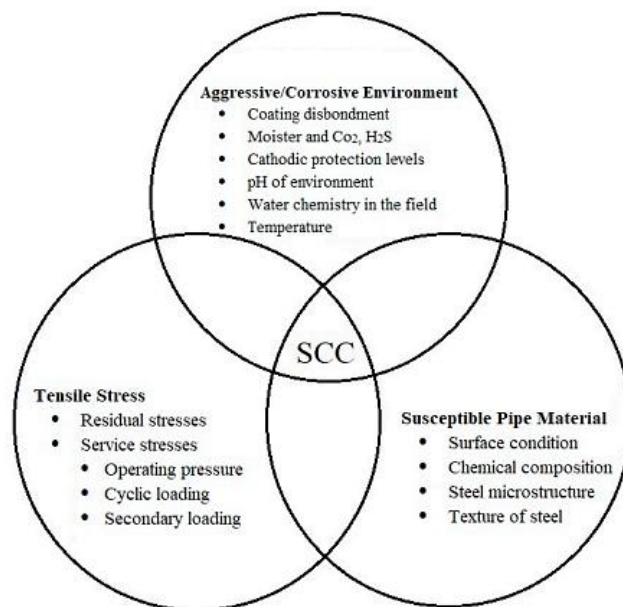


- The pressure and tensile armours are made of carbon steel.
- Mechanical properties and corrosion resistance are key factors in their performance under aggressive environments.

INTRODUCTION



Among the most relevant degradation mechanisms in these systems is CO₂-induced stress corrosion cracking (**SCC-CO₂**).



(MOHTADI-BONAB, 2019)

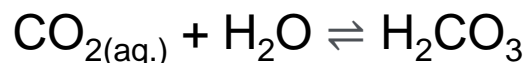
Stress corrosion cracking is a **time-dependent process** in which a metal or alloy undergoes premature cracking due to the synergistic action of a corrosive environment and static tensile stresses—whether applied or residual. Neither the corrosive environment nor the stress alone is sufficient to cause SCC.

A technically significant incident was reported by the Brazilian National Agency of Petroleum, Natural Gas and Biofuels (ANP) in 2017: a flexible gas injection riser failed due to CO₂-SCC just **two years after installation**, despite a projected service life of **20 years**. The failure, which occurred in the tensile armor wires, was caused by the ingress of water and CO₂ into the annular space of the riser.

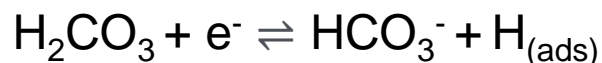
INTRODUCTION



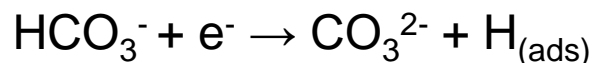
In environments containing CO₂, the formation of protective iron carbonate (FeCO₃) layers on the surface of carbon steels is common. These layers act as barriers that reduce the contact between the metallic substrate and the aggressive environment, thereby contributing to the mitigation of generalized corrosion.



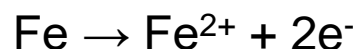
Reaction 1



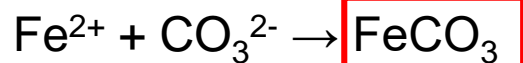
Reaction 2



Reaction 3



Reaction 4



Reaction 5

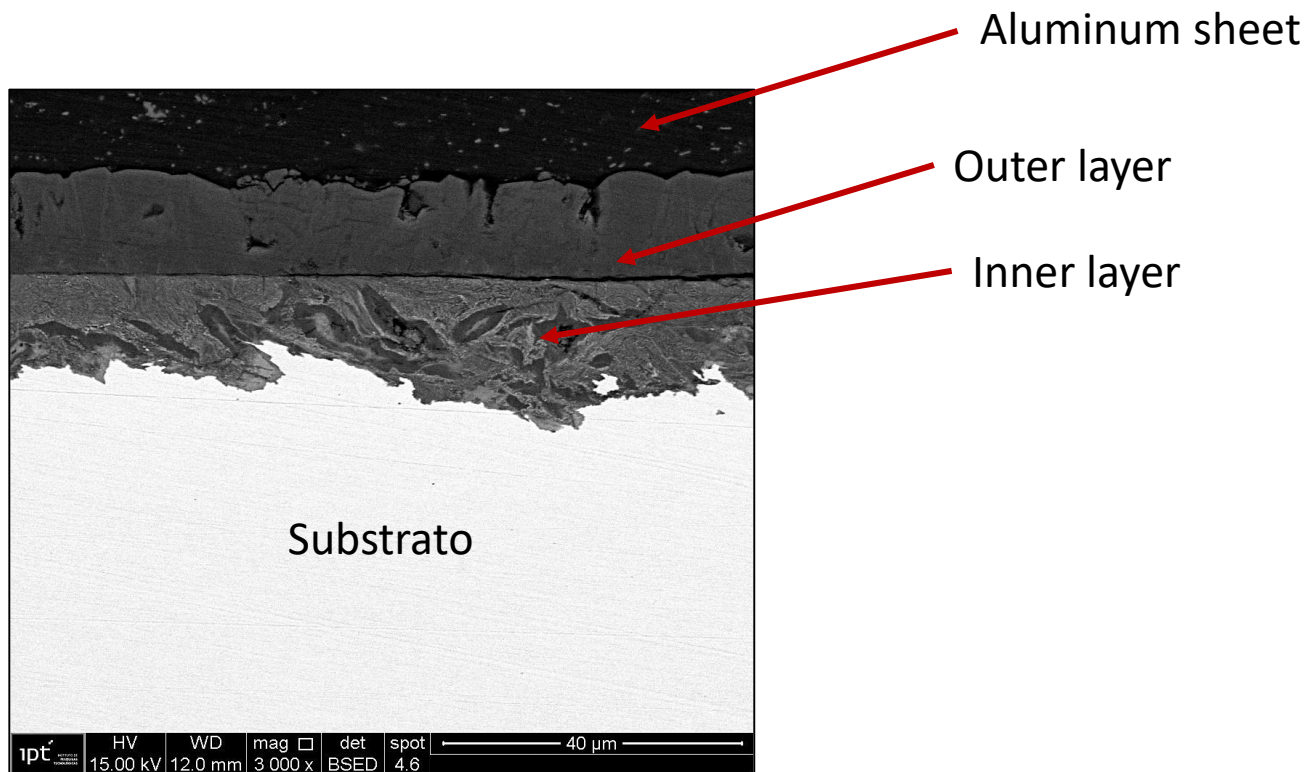
The effectiveness of this protection depends on factors such as the morphology, thickness, adhesion, and integrity of the layer. Adhesion, in particular, plays a key role in the stability of the layer under mechanical stresses: poorly adhered films tend to delaminate, exposing the substrate to corrosive attack.

INTRODUCTION



Siderite formation on carbon steels occurs in two main morphologies:

- an outer crystalized layer and
- an inner compact layer

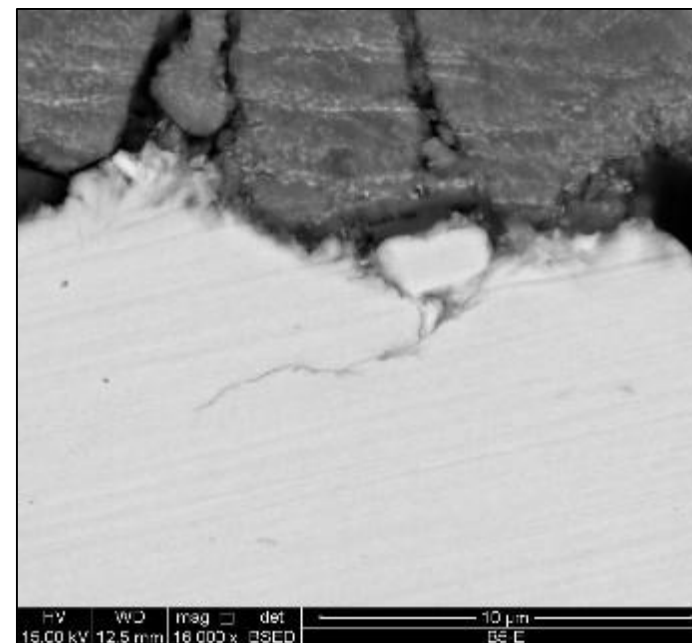
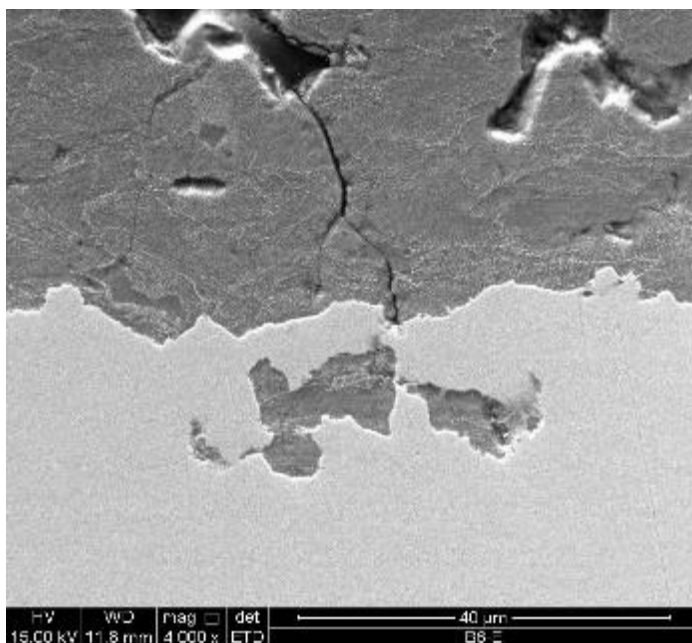


Slide 6/23

INTRODUCTION



In the CO₂-SCC failure mechanism, localized rupture of the FeCO₃ film allows for localized acidic attack, promoting crack nucleation. Additionally, the deformation imposed to elongate the specimen may cause the corrosion product layer to rupture at random locations, exposing the underlying metal to the electrolyte, which is the necessary condition for stress corrosion cracking to occur (PIMENTEL et al., 2025).



Slide 7/23

OBJECTIVE



The objective of the present study is to evaluate the influence of the microstructure of different carbon steels on the formation of iron carbonate (FeCO_3) layers in environments containing carbon dioxide (CO_2).

METHODOLOGY



Five carbon steels commonly used as tensile armor wires in flexible pipes were selected. All exhibit a ferritic-pearlitic microstructure, although with some key differences:

Steel A: low-carbon steel (0.3 %) with a predominantly ferritic microstructure and the presence of spheroidized cementite.

Steel B: steel with a carbon content between 0.6 % and 0.7 %, featuring spheroidized cementite.

Steel C: steel with a carbon content between 0.6 % and 0.7 %, predominantly composed of lamellar pearlite.

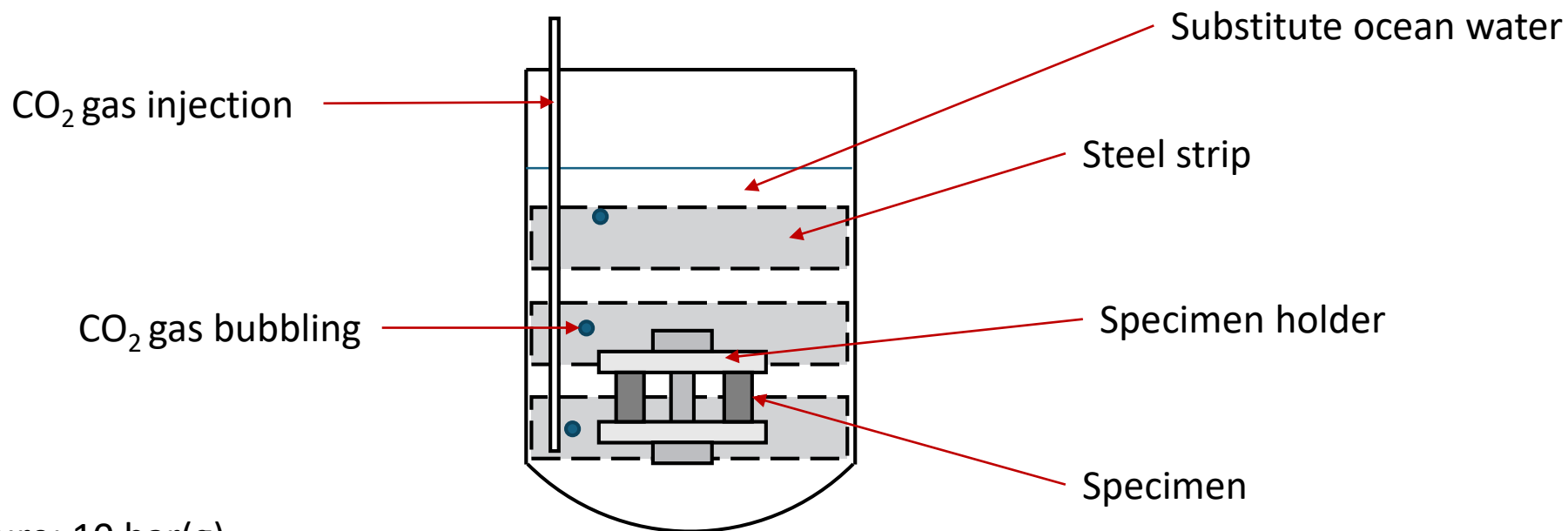
Steel D: steel with a carbon content between 0.73 % and 0.77 %, containing spheroidized cementite.

Steel E: steel with a carbon content between 0.73 % and 0.77 %, primarily composed of lamellar pearlite.

METHODOLOGY



Autoclave test setup



- CO₂ pressure: 10 bar(g)
- Temperature: 40 °C
- Relation volume/area (V/A): 1 mL/cm²
- Duration: 47 days

Slide 10/23

METHODOLOGY



The specimens were ground, finishing with **#600 grit** sandpaper, ensuring that the grinding marks were aligned with the **drawing direction** of the specimens — matching the direction of the surface marks produced during the wire drawing process.

For characterization, the following procedures were performed:

- Tensile tests: three tests per material;
- Chemical composition determined by optical emission spectrometry (OES);
- Microstructure evaluated by scanning electron microscopy (SEM).

METHODOLOGY



Due to the cross section geometry of the wires, the areas marked in green, as schematically shown below, were selected for evaluation. SEM was used to measure the thickness of all iron carbonate layers (inner, outer, and total).

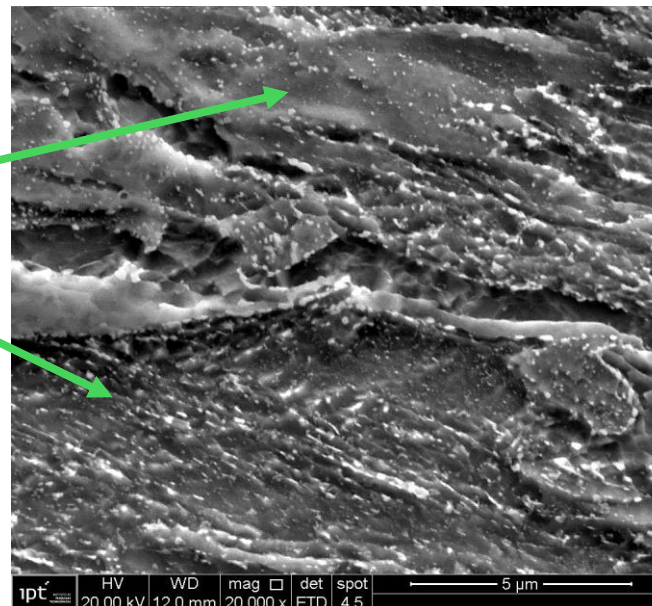


For each evaluated area, three regions were selected (one central and two at the edges) for measurements, with five measurements performed in each region. Thus, for each specimen, a total of 30 measurements were conducted per layer.

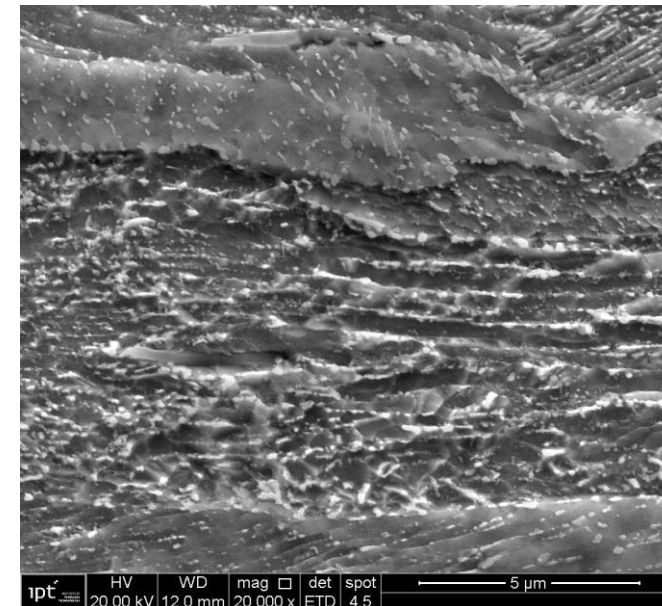
RESULTS

Steel A

Ferrite
 Spheroidized cementite



Cross-section



Longitudinal

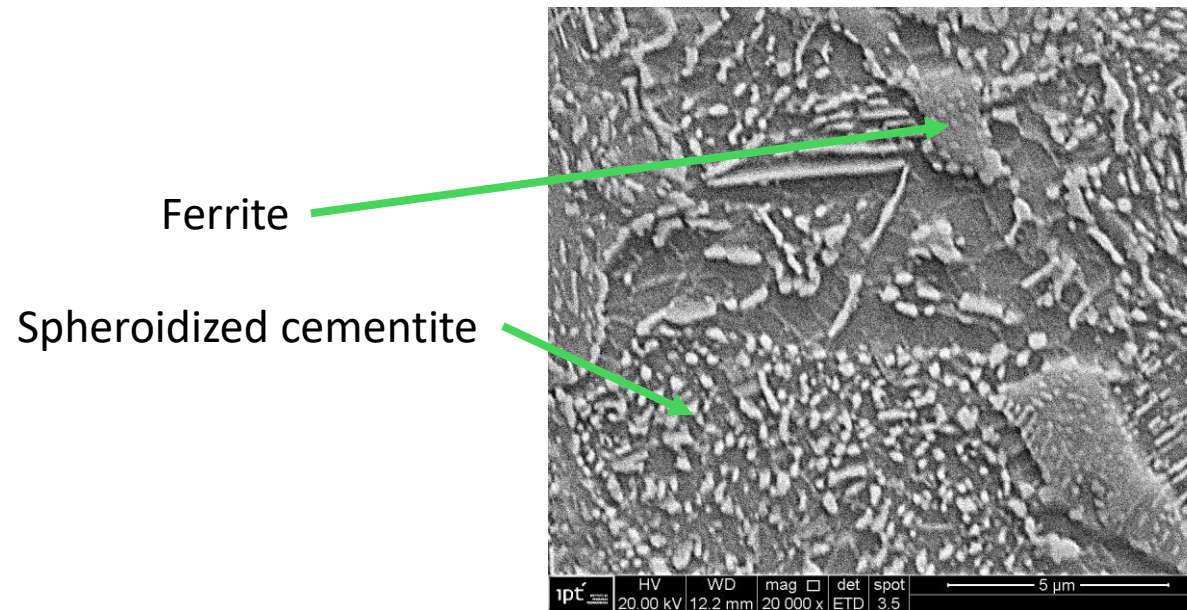
Material		Modulus of Elasticity [GPa]			Yield strength, 0.2 % [MPa]			Ultimate tensile strength [MPa]			Total elongation at fracture [%]			
Steel A	Mean	169			833			949			12.4			
	Standard Dev.	10			26			11			0.9			
Material		Content (%wt)												
		C	Mn	Si	P	S	Cr	Ni	Mo	Al	Cu	Ti	V	Nb
Steel A		0.330	0.731	0.226	0.011	<0.001	ND	0.001	0.001	0.040	0.004	0.001	0.001	ND

13/23

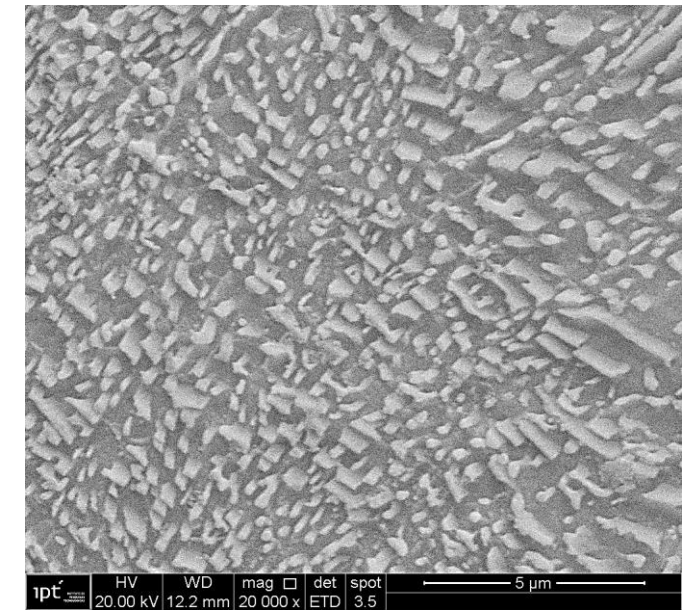
RESULTS



Steel B



Cross-section



Longitudinal

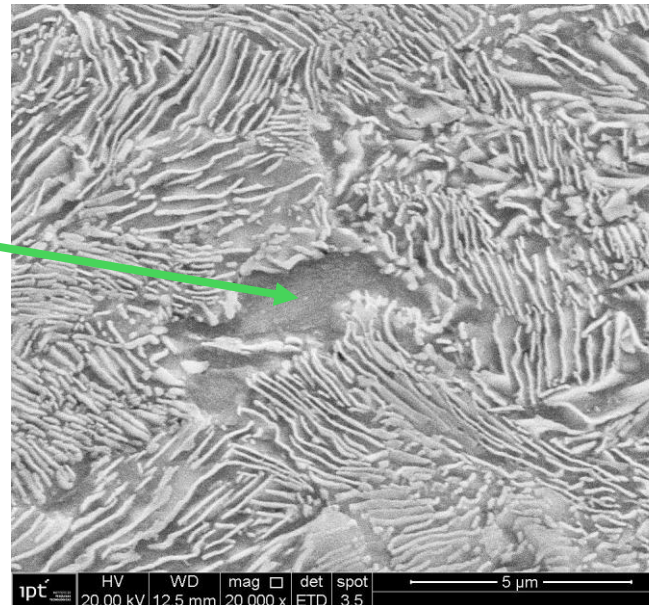
Material		Modulus of Elasticity [GPa]			Yield strength, 0.2 % [MPa]			Ultimate tensile strength [MPa]			Total elongation at fracture [%]			
Steel B	Mean	169			753.2			797.1			15.5			
	Standard Dev.	22			4.4			3.2			1.0			
Material		Content (%wt)												
		C	Mn	Si	P	S	Cr	Ni	Mo	Al	Cu	Ti	V	Nb
Steel B		0.602	0.650	0.280	0.006	<0.001	ND	0.001	0.001	0.041	0.001	0.001	0.002	ND

RESULTS

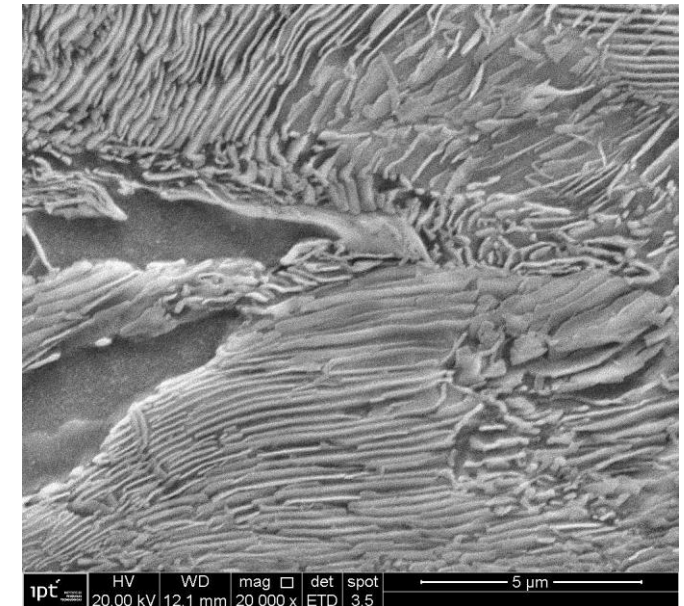


Steel C

Ferrite
 Lamellar pearlite



Cross-section



Longitudinal

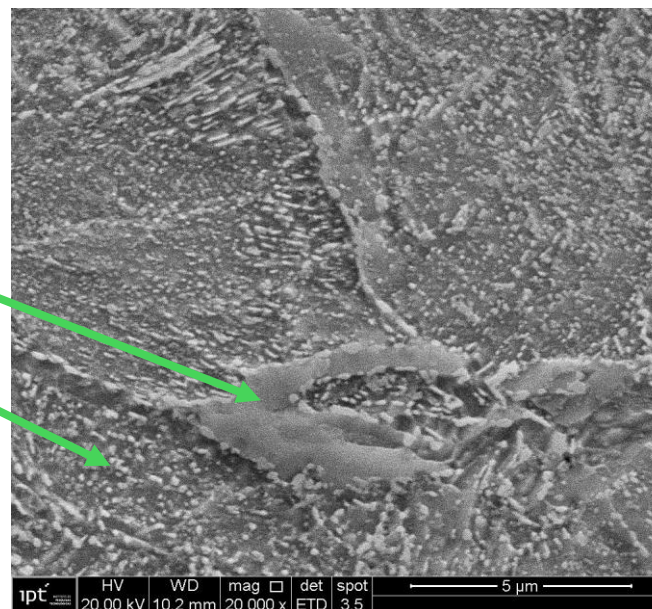
Material		Modulus of Elasticity [GPa]			Yield strength, 0.2 % [MPa]			Ultimate tensile strength [MPa]			Total elongation at fracture [%]			
Steel C	Mean	180.6			1337			1506			4.19			
	Standard Dev.	1.5			68			69			0.25			
Material		Content (%wt)												
		C	Mn	Si	P	S	Cr	Ni	Mo	Al	Cu	Ti	V	Nb
Steel C		0.682	0.661	0.229	0.004	<0.001	ND	0.001	0.001	0.030	0.007	0.001	0.003	ND

RESULTS

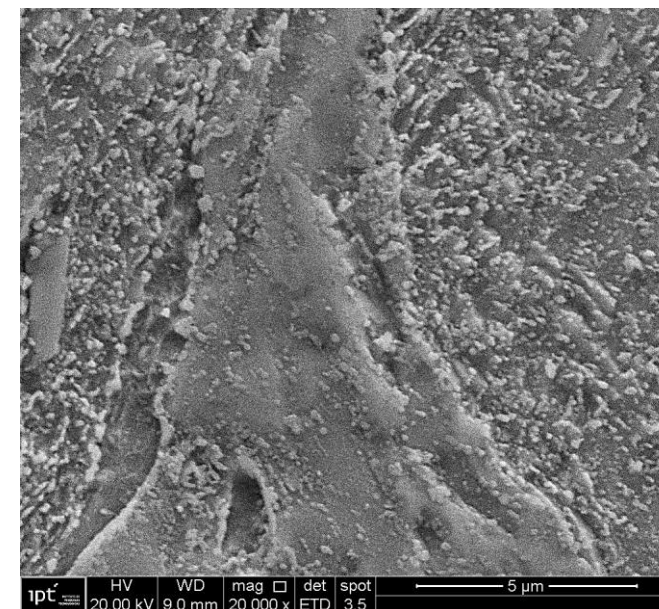


Steel D

Ferrite
 Spheroidized cementite



Cross-section



Longitudinal

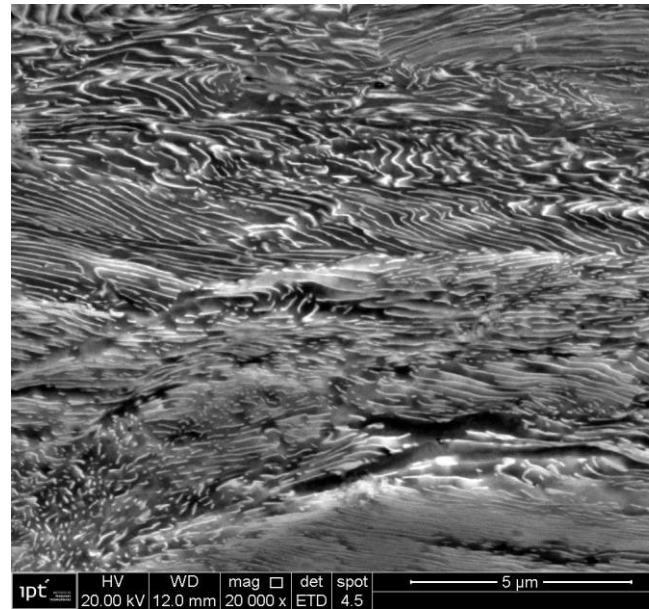
Material		Modulus of Elasticity [GPa]			Yield strength, 0.2 % [MPa]			Ultimate tensile strength [MPa]			Total elongation at fracture [%]			
Steel D	Mean	222			1160.3			1273.4			9.4			
	Standard Dev.	16			4.9			3.8			1.1			
Material		Content (%wt)												
		C	Mn	Si	P	S	Cr	Ni	Mo	Al	Cu	Ti	V	Nb
Steel D		0.732	0.811	0.241	0.008	<0.001	ND	0.001	0.001	0.029	0.008	0.001	0.002	ND

RESULTS

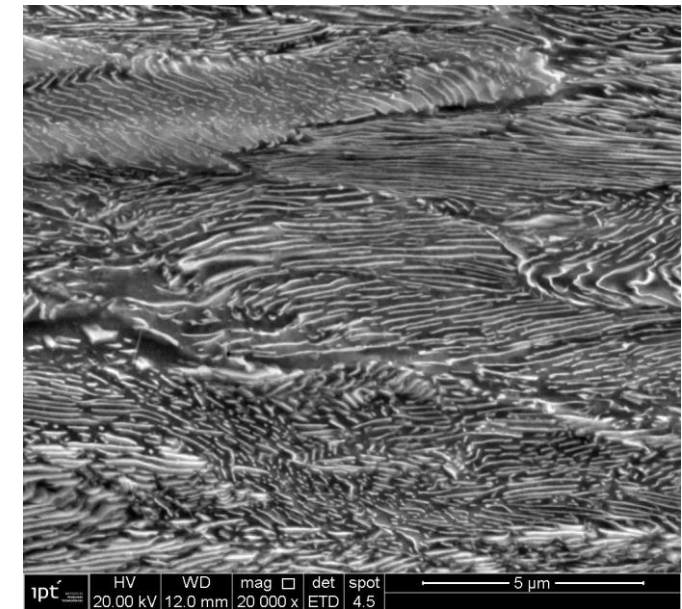


Steel E

Predominantly lamellar pearlite



Cross-section

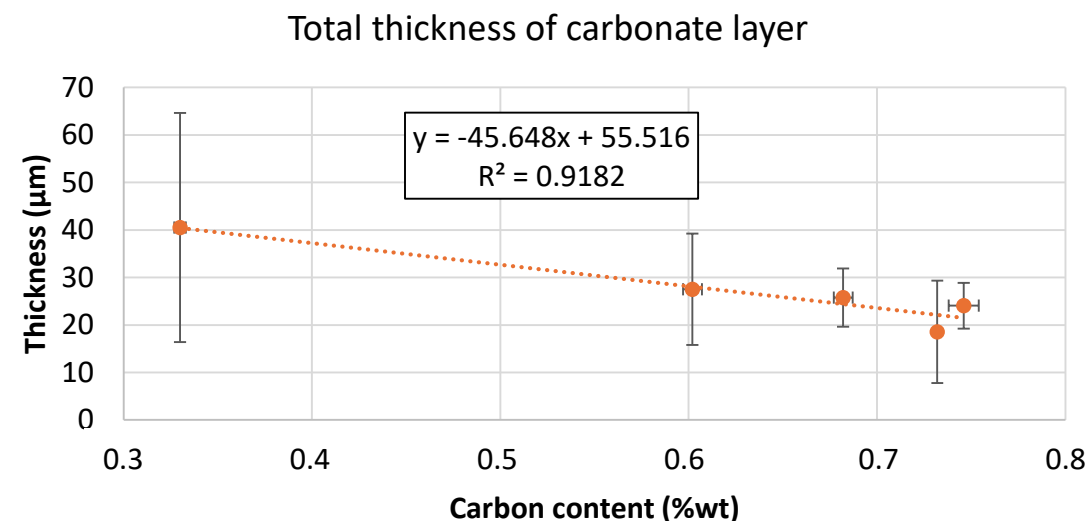
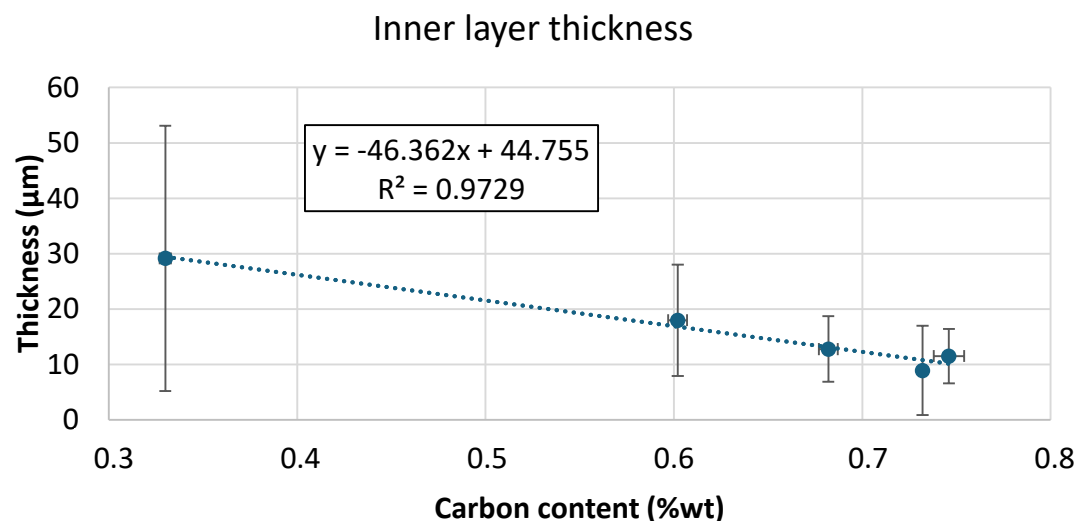


Longitudinal

Material		Modulus of Elasticity [GPa]			Yield strength, 0.2 % [MPa]			Ultimate tensile strength [MPa]			Total elongation at fracture [%]			
Steel E	Mean	166			1300			1505			5.1			
	Standard Dev.	70			30			40			1.3			
Material		Content (%wt)												
		C	Mn	Si	P	S	Cr	Ni	Mo	Al	Cu	Ti	V	Nb
Steel E		0.746	0.775	0.278	0.013	0.015	0.028	0.001	<0.002	0.001	0.024	0.002	0.002	0.002

RESULTS

Relationship between carbon content and the inner layer thickness

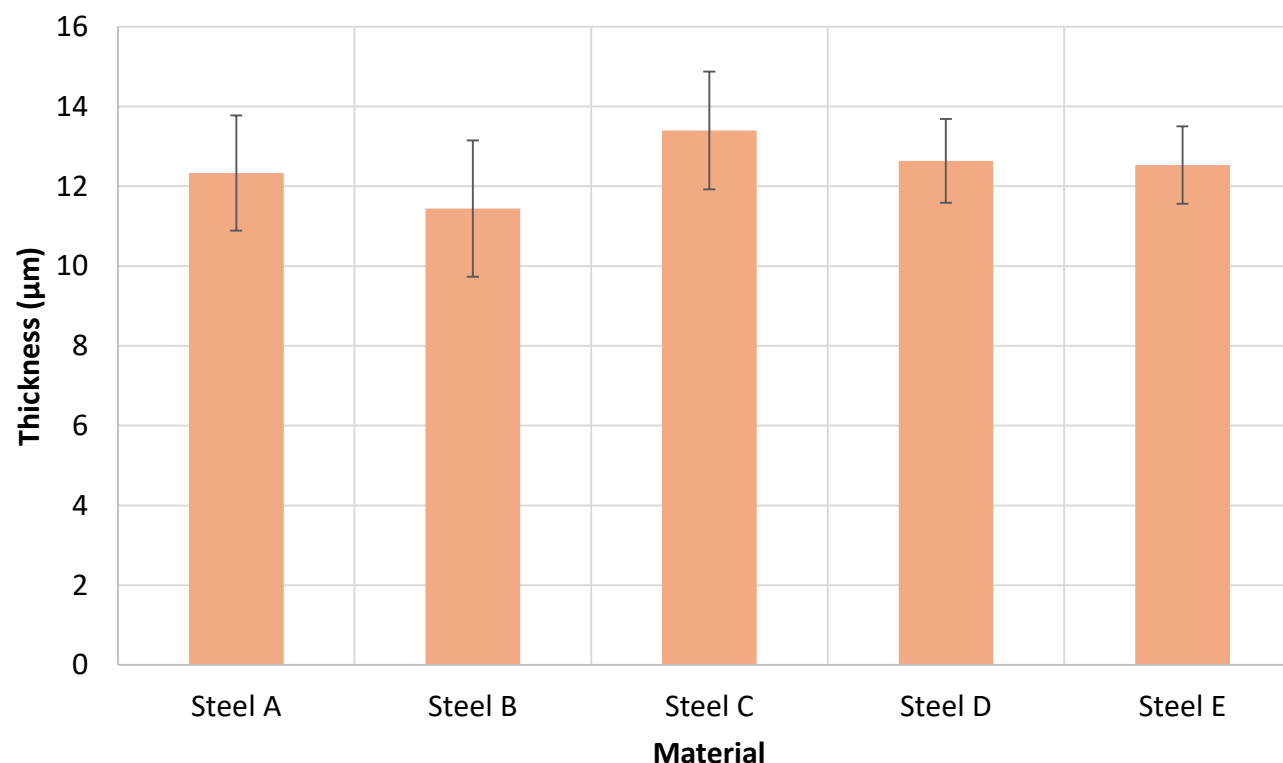


- There is a tendency for the thickness of the inner carbonate layer to decrease as the carbon content increases.
- The standard deviation values also tend to decrease with increasing carbon content.

RESULTS



Outer layer thickness



According to the analysis of variance (ANOVA), the values are statistically different (p -value of 2.65×10^{-5}), with no clear trend in the measurement behavior.

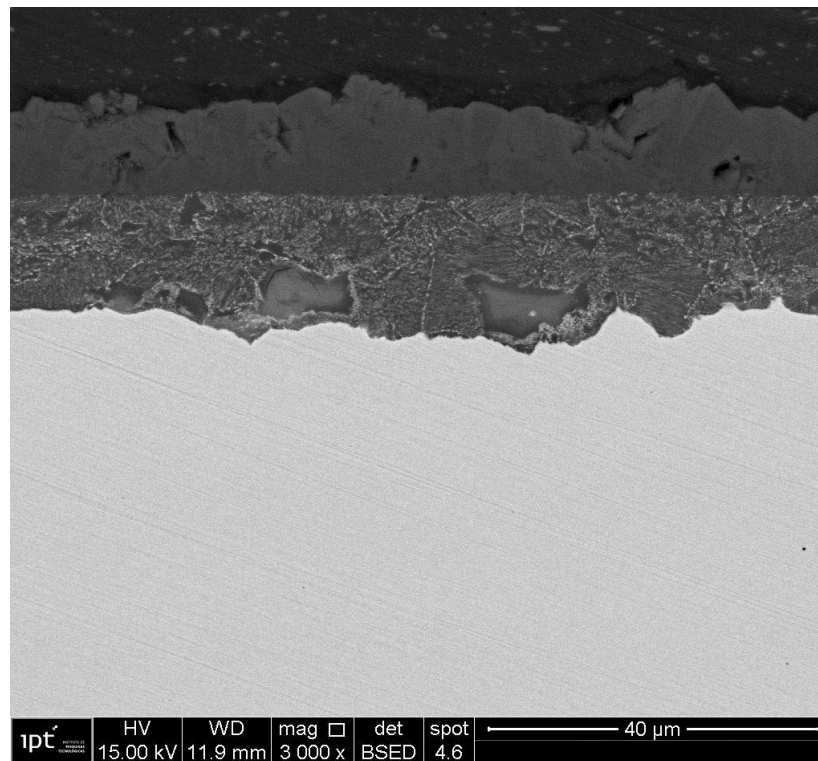
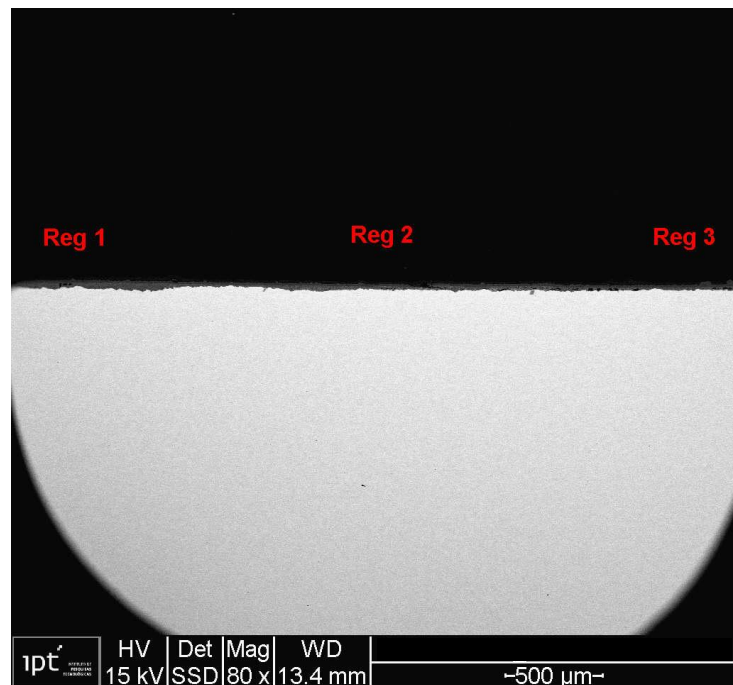
However, when compared with the thickness values of the inner layer, this difference becomes negligible.

In the spheroidized steels, regions were identified where the outer layer was not present.

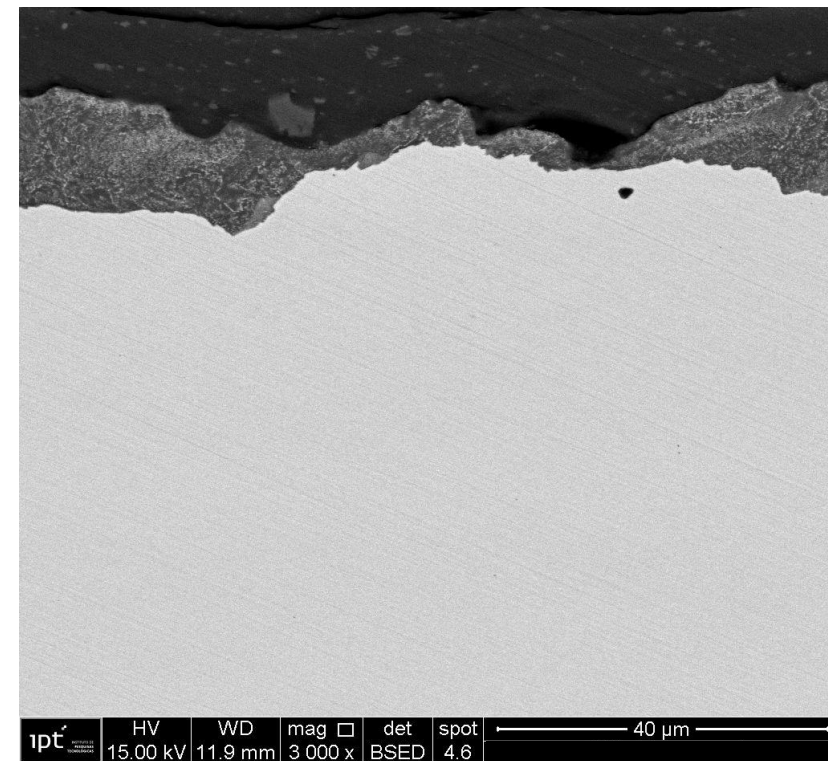
Slide 19/23

RESULTS

Steel B



Reg. 2

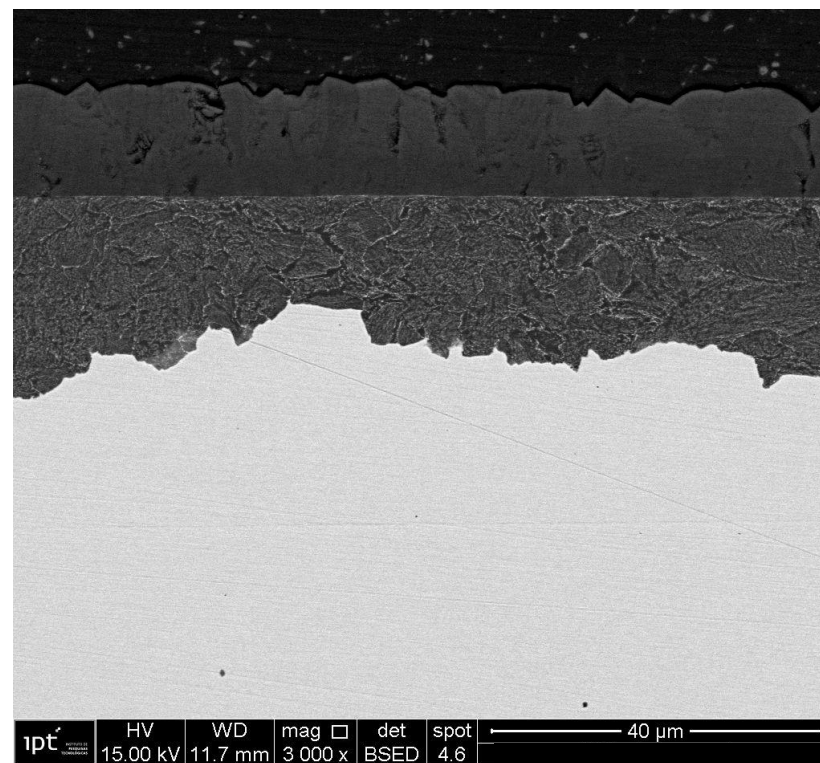
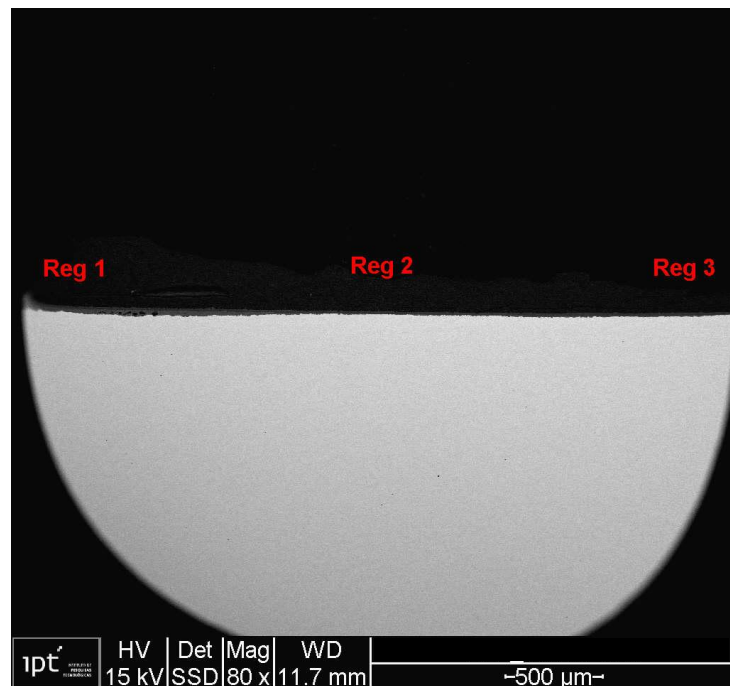


Reg. 3

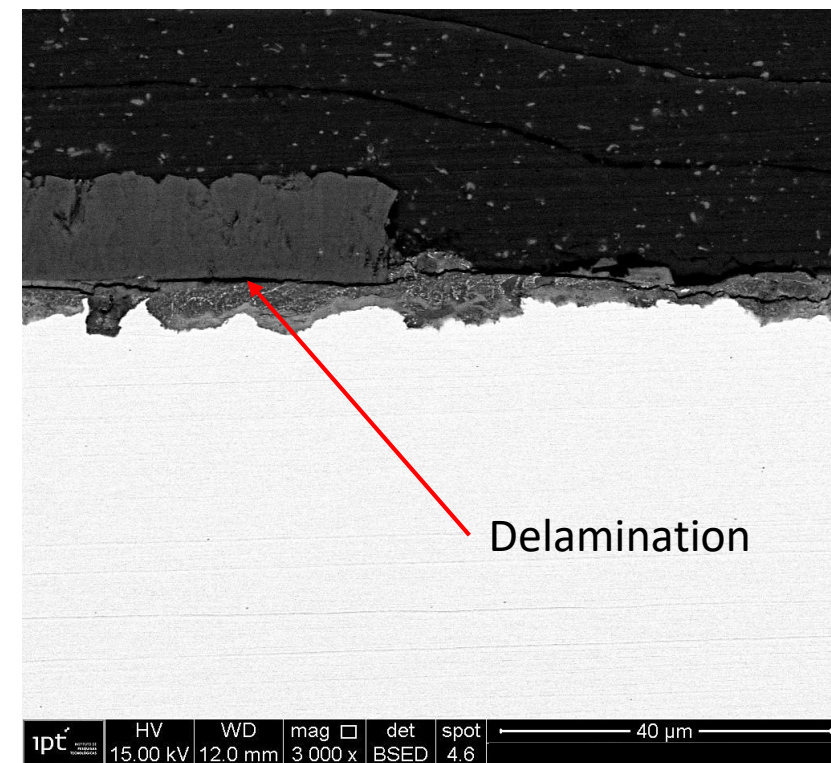
During the test, the outer layer detached from the specimen surface

RESULTS

Steel D



Reg. 1



Reg. 2

The spheroidized microstructure provided poorer mechanical support for the outer layer, leading to adhesive failure.

Slide 21/23

CONCLUSIONS



- The effect of carbon content on the thickness of the outer iron carbonate layer showed statistically significant differences according to ANOVA; however, when compared to the total thickness of the complete carbonate layer, its effect is negligible.
- An increase in the carbon content of the evaluated hypoeutectoid steels led to a reduction in the thickness of the inner iron carbonate layer.
- The outer carbonate layer of steels with a higher proportion of spheroidized pearlite provided poorer mechanical support, as evidenced by the presence of cracks and delamination.

FUTURE WORK



Adhesion evaluation

- Instrumented nanoindentation tests
- Continuous scratch tests to assess adhesion between layers

Carbon content effect

- Repeat the same tests on lower carbon steels (e.g., steels used in rigid pipes)

Environmental parameters

- Study the effect of CO₂ partial pressure and exposure time on the morphology and properties of iron carbonate layers



THANK YOU!